Thin–Walled Structures xxx (xxxx) xxx

Contents lists available at ScienceDirect

Thin-Walled Structures

journal homepage: http://www.elsevier.com/locate/tws

Corrected method for scaling the dynamic response of stiffened plate subjected to blast load

Xiangshao Kong [a,b], Hu Zhou [a], Zheng Kuang [a], Cheng Zheng [a,*], Xiao Li [c,**], Weiguo Wu [a], Zhongwei Guan [b]

[a] Departments of Naval Architecture, Ocean and Structural Engineering, School of Transportation, Wuhan University of Technology, Wuhan, 430063, China
[b] School of Engineering, University of Liverpool, Liverpool, L69 3GH, UK
[c] Department of Maritime and Transport Technology (M&TT), Delft University of Technology, Netherlands

ARTICLE INFO

Keywords:
Corrected similarity relationship
Dynamic response
Stiffened plate
Double geometric parameters distortion
Numerical simulation
Confined blast load

ABSTRACT

Test on a small scaled model is an effective approach to predict the dynamic response of full scale structure under blast loadings. However, the geometric dimensions of specimens cannot simply comply with complete geometrical similarity due to manufacture or test restrictions. It would result in the difference structural performance between the full and small scaled models. This paper proposed a corrected similarity relationship of the dynamic behaviour between prototype and replica of stiffened plates subjected to blast load, in which both the thickness of the plate and the configuration (cross-sectional shape) of stiffeners are distortedly scaled-down (double distorted geometric scaling factors). Firstly, based on the mesh convergence study and comparing with results from experimental tests, a numerical method in predicting the confined blast load and dynamic response of structure was verified, which provides a reliable means to determine the dynamic behaviour of stiffened plate designed by the corrected similarity criterion of this paper. Then, the influence of altering the stiffener configuration on the dynamic response of stiffened plates was analysed and on the basis of it, a criterion for scaling the stiffener is proposed to help design a stiffener-distorted model from prototype structure. In addition, a method for scaling the double-parameter distortedly small scaled model is proposed to predict the dynamic response of the prototype. Finally, two sets of examples of both the small size and prototype stiffened structures subjected to blast load were analysed by using the presented method. It is shown that the replica developed by applying the present method is able to accurately predict the behaviour of the full-size stiffened plates, even when the thickness of the plate and the configuration of the stiffeners are distortedly scaling down with different factors.

1. Introduction

Blast loading produced by an accidental or intentional explosion, such as gas explosion in inner buildings, missile attack in a combat environment or terrorist attack on airplanes and public facilities, may provoke not only permanent damage to structures but also degradation of the environment and human losses [1,2]. Stiffened plates have been widely used as basic unit in thin-wall structures, such as ship hull and airplane constructions. A better understanding of the dynamic response of a stiffened plate subjected to blast loading would help design the structures with enhanced blast resistance and increase the level of safety for personnel and structures in increasingly threatening environments. Identifying the best way to investigate the shock response of these structures under blast loading has always been a challenge task. Researchers and designers have been of particularly concerning the dynamic responses and damage of structures under extremely server loading conditions [3–11]. It is believed that the full-scale experiment is the most reliable method of evaluating the anti-blast performance of structures, but with the huge expenditure and environmental conditions imposed restrictions on any successive tests. Testing of small scaled models is nowadays still a valuable design tool, helping researchers to accurately predict the behaviour of oversized prototypes through scaling laws applied to the experimental results [5,12–17] obtained.

However, several limitations and difficulties still persist when applying the similitude theory through the current methodologies to

* Corresponding author.
** Corresponding author.
E-mail addresses: zhengchengyeep@whut.edu.cn (C. Zheng), X.Li-9@tudelft.nl (X. Li).

https://doi.org/10.1016/j.tws.2020.107214
Received 17 June 2019; Received in revised form 25 August 2020; Accepted 14 October 2020

Nomenclature

Roman symbols

C	constant for $C = (\lambda_h)^{n_{I_1}}$
h	thickness of the plate
I	impulse per unit area of shockwave
I_j	moment of inertia
L	length
l_1, l_2	distance from the centroid of compression and tension area to the neutral axis of the cross-sectional area of stiffener, separately
M_0	plastic limit bending moment
N_0	plastic limit neutral plane force
n_0	number of stiffeners
n_I	exponent
R	stand-off distance
S_1, S_2	static moment from the compression and tension area to the neutral axis of the cross-sectional area of stiffener, separately
S_j	cross sectional area
t	time
v	velocity
W	mass of explosive
W_j	section modulus
w	deflection of the plate

Greek symbols

β	scaling factor
β_x	factor of distorted geometric parameter x
λ_x	factor of distorted geometric parameter x
π	dimensionless number
ρ	material density
σ_0	static yield stress
σ_d	dynamic yield stress

Superscripts

$(\,)^m$	small scaled model (reference model)
$(\,)^p$	prototype
$(\,)^c$	correction model

blast loaded structures. Firstly, the dynamic response of scaling structures hardly follows the general similarity laws if they were built with materials that sensitive to strain-rate. Secondly, due to manufacturing technical restrictions, the configuration of small scaled models cannot comply with the prototype completely in an overall scaling factor. In that case, some geometrical parameters of a small scaled model have to be altered to meet the demand of experiments due to the limitations. The two factors mentioned above would result in incomplete similarity between the small scaled model and the prototype in practice. Much work [18–24] have been undertaken on the similarity relationship of the dynamic responses between the incomplete small scaled model structure and the prototype under impact or blast loads.

For the process of structural impact events involves plastic flow and possible local material fracture [25], the influences of strain-rate strengthening effect on the dynamic yield stress are remarkable. Therefore, it is still a difficult task in solid mechanics to establish the strain-stress relationships [26,27]. How to deal with the influence of the material nonlinearity on the complete similarity remains a major challenge. The distorted configuration of small scaled models has been posed as the main limitation for traditional or non-corrected scaling laws in blast or impact scenarios, along with other limitations such as strain-rate and inertia effects [16]. Oshiro and Alves firstly proposed a Non-Direct Similitude technique [18,28,29], which was used to skilfully address the strain-rate effect on the dynamic yield stress by changing the impact velocity. This technique provided a reliable and effective method to predict dynamic responses of a structure subjected to impact or blast loading by using test results of a small size replica. Furthermore, they successfully predicted the dynamic response of prototypes by using small scaled models that made of different materials or with distorted configurations [19,30]. Luo et al. [31,32] conducted a numerical study on the scaling of a rotating thin-wall short cylindrical shell. Sensitivity analysis and governing equations were employed to establish the scaling law between the distorted model and the prototype, which was aimed to provide an effective scaling law, applicable structure size intervals and boundary functions that could guide the design of distortion models. Cho et al. [33] presented the research on the similarity method based on two kinds of scaled models, one with distorted configurations and the other made of another material. This study was to overcome the dimensional and material limitations in model tests and predict the dynamic response of the prototype by combining the two distorted factors mentioned above. Yao et al. [34] performed an investigation of scaling the deformation of steel box structures subjected to internal blast loading experimentally and numerically. In addition, correction of the scaling law for steel box structure was conducted which considered both the scale-down factor and the scale strain-rate effect. In our previous work [35], a corrected similarity relationship between the incomplete small scaled model and the prototype of blast loaded structure was proposed, in which only one geometric parameter of the model was distortedly scaled.

However, another problem arises when more distorted factors needed to be taken into account in the design of the small scaled model, such as multi-stiffened plates. Stiffeners on the plate play an important role in energy absorption and blast resistance of the whole structure. Owing to manufacturing technical restrictions, the distorted small scaled factors of both the thickness of the plate and the size of stiffeners do not comply with the overall geometric scaling factors. Also, the configuration of stiffeners needs to be further altered to meet the requirement of fabrication of experimental sample structures. Here, the configuration change of stiffeners in a small scaled model is referred to as the stiffener-distorted model.

A corrected similarity relationship for predicting the dynamic response of stiffened plates subjected to blast loads is proposed by using a small scaled model. Here, geometric distorted small scaled models are used, in which both the thickness of plates and stiffener configurations are distorted. The study includes the development of the distortion criterion of stiffener types that is valid when replace the T-type stiffener with the flat bar, followed up with a similarity relationship for predicting the dynamic response of the prototype. Two analytical examples are introduced to verify the reliability of this similarity method by employing a verified numerical method.

2. Numerical simulation method of the blast load and response of structure

In order to provide a reliable means to determine the dynamic behaviour of stiffened plate designed by the corrected similarity criterion of this paper, in this section, the verification of numerical simulation method in predicting the blast load and dynamic response of stiffened plate was performed. Firstly, mesh convergence studies in calculating the confined blast load in 2D and 3D space were performed. Then, the numerical method in predicting the confined blast load and the deflection of stiffened plates were compared with the measured data from experiments. The schematic diagram of the experimental device is shown in Fig. 1. It is a hollow cuboid with a venting hole on one side. The

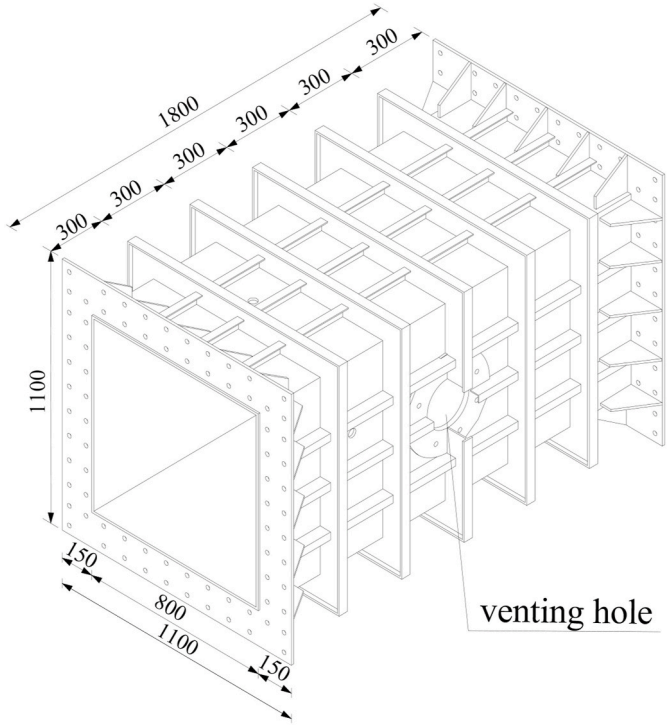

Fig. 1. Sketch of the experimental setup (all dimensions in mm).

explosive was placed in the middle of this cuboid box and two specimens of stiffened plates are fixed to the each end of this test device [36].

A numerical simulation method was employed to predict the confined blast load and subsequent dynamic response of a stiffened plate by employing ANSYS AUTODYN. In experimental tests, cylindrical explosive charges with different masses and dimensions were used to produce the blast loads. The dimensions of the cylindrical explosive charge are quite smaller than that of the blast test chamber and stiffened plates, so the remapping capability in AUTODYN was employed to reduce the computational cost associated with the initial stages of the calculation which involves the detonation and expansion of the cylindrical explosive charge. In order to provide the more accurate confined blast loading with relative low computational costs, the pressure field within the chamber was produced by mapping in the pressure field resulting from a 2D simulation. The region inside the blast chamber, which includes air and explosive charge, was firstly modelled using the multi-material Euler formulation in AUTODYN-2D, as shown in Fig. 2. The cylindrical TNT enables the 2D axial symmetry condition to be used. Due to the mesh size has an influence on the blast load, the mesh sensitive studies were firstly performed by discretizing the 2D computational domain with different sizes of mesh. Three gauges were placed

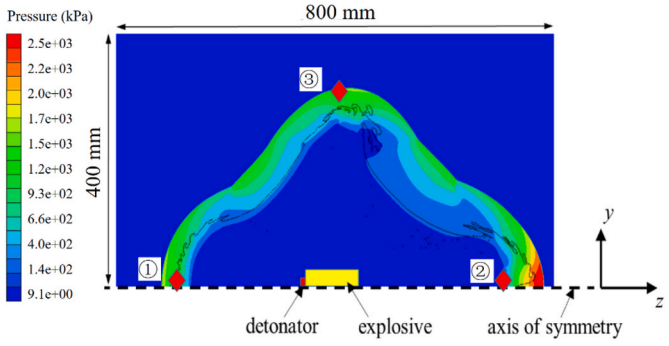

Fig. 2. 2D FE model for blast wave calculation.

100 mm away from the corresponding boundary edges to compare the pressure change in conditions of different mesh sizes. In this paper, 8 numerical calculations with different mesh sizes were performed, in which square grids were used with thickness of 1.33, 1.00, 0.80, 0.67, 0.57, 0.50, 0.44 and 0.40 mm, respectively.

In the numerical simulations, the Jones-Wilkins-Lee (JWL) Equation of State (EOS) was implemented to describe the explosive materials, which is defined as,

$$p = C_1\left(1-\frac{w}{r_1 v}\right)e^{-r_1 v} + C_2\left(1-\frac{w}{r_2 v}\right)e^{-r_2 v} + \frac{wE}{v} \tag{1}$$

In addition, the air is modelled with an ideal gas equation of state as follows,

$$p = (\gamma - 1)\rho e \tag{2}$$

where $\gamma = 1.4$ is the heat specific ratio, $\rho = 1.225\ \mathrm{kg/m^3}$ is density, $e = 2.068 \times 10^5\ \mathrm{J/kg}$ is internal energy, $C_1 = 3.7377 \times 10^5$ MPa, $C_2 = 4.15$, $r_1 = 3.75 \times 10^3$ MPa, $r_2 = 0.9$ are constants, $\omega = 0.35$ is the specific heat, v is specific volume.

The 2D simulation is terminated before the shockwave reached the nearest edge of the computational domain. The peak pressures from the three gauges are collected and compared to investigate the influence of mesh size on the calculated shock wave, as shown Fig. 3, in which the pressure change represents the comparison of peak pressure between the fine mesh and the coarse mesh. It is found that the finer mesh is more capable in capturing the peak value of more intensified shock wave, but more time consuming. Due to the factor that the size of 2D computation domain is only 400 mm × 800 mm, the mesh size of 0.4 mm × 0.4 mm is adopted in the numerical simulations.

After the pressure distribution in 2D domain is obtained, it was remapped into 3D space of the blast chamber, of which the dimensions of length, width and height are 1800 mm, 800 mm and 800 mm, respectively. It is almost impossible to implement the numerical calculations by employing the same mesh size with that of in 2D computational domain. In order to find out a suitable model with acceptable accuracy in predicting the confined blast load, the grid sensitive is also studied for the 3D computational domain. The symmetry of the problem under consideration allows modelling only half of the whole inner space of blast chamber, as shown in Fig. 4. The dimensions of the computational domain are 900 mm, 800 mm and 800 mm, and four different sizes are used in the conditions of 55 g TNT and 110 g TNT, respectively. In the numerical calculations, 8 pressure gauges were arranged at different location of the boundary wall, and the detailed data of gauges

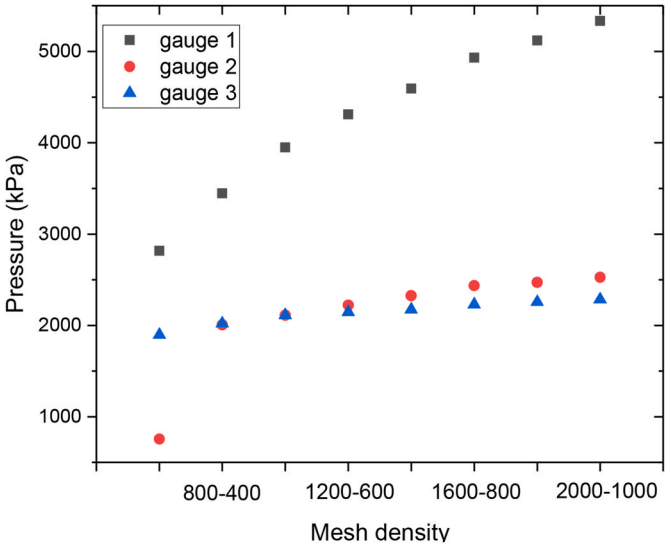

Fig. 3. Relationship between the mesh density and the peak pressure.

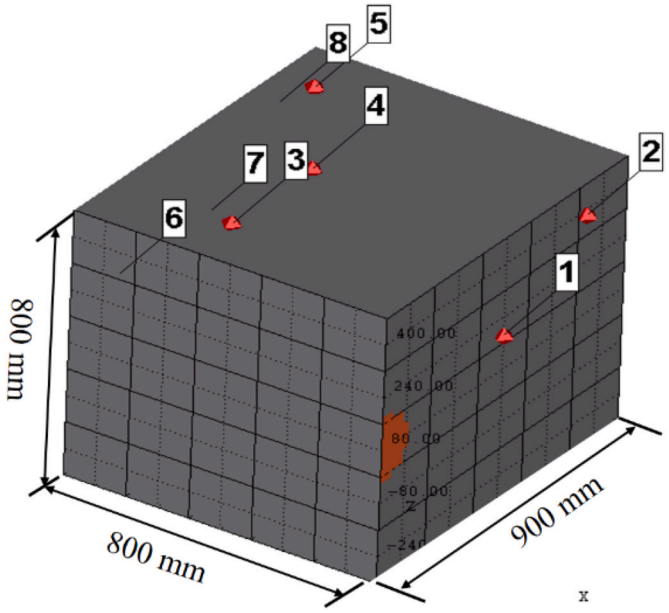

Fig. 4. Three dimensional model and locations of pressure gauges.

2, 4 and 5 were plotted in Fig. 5(a) and (b), in which the relationship between the mesh density and peak pressure of the calculated shock wave in conditions of 55 g TNT and 110 g TNT were reflected, respectively. The comparison shows that when the mesh density was refined from 90 × 80 × 80 to 112 × 100 × 100, the peak pressure was increased by the maximum value of 3.26% and 2.57% among three gauges in conditions of 55 g TNT and 110 g TNT, respectively. However, the computational cost was increased by 66%. By considering the balance between efficiency and accuracy, the mesh density of 90 × 80 × 80 is selected in the numerical model, resulting in a total number of 576,000 grids. Furthermore, as the remapping method is employed, the size of the explosive in the 2D domain would have a slight influence on the calculated blast load in the 3D space. Besides, according to the Hopkinson scaling law, mass, distance and time can be scaled for explosives over a wide range of charge sizes [37], so that testing can be conducted at a laboratory scale and results can be extrapolated to a large scale, reducing the need for full-scale tests. The small scaled and prototype of explosions have the same peak value of overpressure, and the duration time of shock wave is scaled down with the same factor as the geometrical scaling factor. Besides, the responses of stiffened plate under confined blast load are usually impulse dependent [38], which is less sensitive to the peak value of overpressure of shockwave in confined blast. Thus, in the numerical calculations of dynamic responses of stiffened plates subjected to confined blast load, the mesh sizes of both the prototype and the small scaled models of 3D computational domain could remain unchanged.

The above verified numerical model is used to calculate the blast load in a partly confined chamber and the results are compared with the measured data from experiments in Fig. 6. It is shown that the numerical simulation method is capable of predicting the initial shock wave and rebounded shock wave from walls of chamber, which would provide a relative accurate input load in the prediction of dynamic responses of blast loaded stiffened plates.

Based on the calculation of blast load in confined chamber, the 3D numerical simulations of the dynamic response of steel plate subjected to confined explosion, in which the Fluid-Structure Interaction (FSI) process was taken into account to implement the coupling between the confined blast load and the steel plate, were further conducted. Generally, structures can be defined in a Lagrangian reference frame where the mesh follows the material movement, and the Eulerian reference is a more preferable method to describe the gas flow from detonating explosives. In the present study, the air is modelled with Euler elements which is an extension of Eulerian approach, while the steel plates were modelled with Belytschko-Tsay shell elements based upon Mindlin theory [39]. The air domain in the numerical model should be large enough to cover the deformed plates. Besides, an additional space was provided for the high pressure air blow out from the venting hole in the wall of experimental setup, as shown in Fig. 1. Thus, the whole Eulerian domain of air has a dimension of 2000 × 1600 × 800 mm. The wall including the venting hole is modelled as a rigid material and meshed with 8 node solid elements. The out-flow boundary conditions are set on all finite sides of the Euler grid, except on the three specified surfaces, which represent the rigid walls of the blast chamber, as these are reflective boundaries (no-flow out condition).

A fully coupling algorithm was used to connect the Lagrange solver and Eulerian solver. As the Lagrange body moves, it acts as a moving boundary in the Euler domain by progressively covering volumes and faces in the Euler cells. This induces flow of material in the Euler Domain. At the same time, a stress field will develop in the Euler domain which results in external forces being applied on the moving Lagrangian body. These forces will feedback into the motion and deformation (and stress) of the Lagrangian body. Large deformations may also result in erosion of the elements from the Lagrangian body. The coupling interfaces are automatically updated in such cases. In more detail, the Lagrangian body covers regions of the Euler domain. The intersection between the Lagrangian and Eulerian bodies results in an updated control volume on which the conservation equation of mass, momentum and energy are solved, as shown in Fig. 7. In the numerical simulations, the parameter of "cover fraction limit" in Autodyn is used to determine when a partially covered Euler cell is blended to a neighbour cell, and the value of cover fraction limit was set to 0.5, which means that when

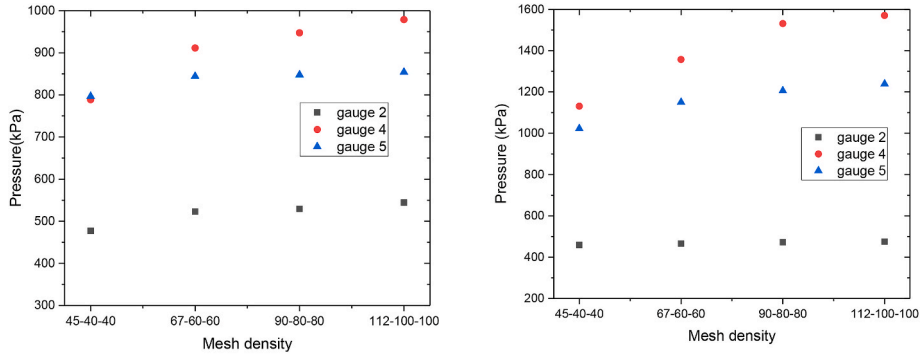

(a) 55 g TNT (b) 110 g TNT

Fig. 5. Relationship between the mesh density and peak pressure of calculated shock wave.

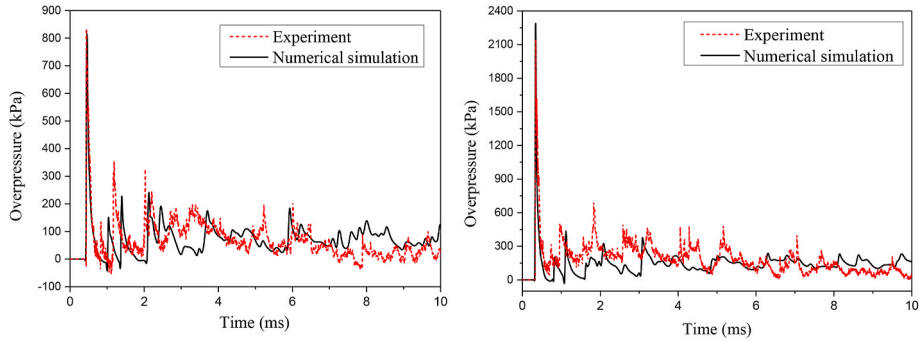

(a) 55 g TNT (b) 110 g TNT

Fig. 6. Comparison of pressure-time histories of experiments and numerical simulations.

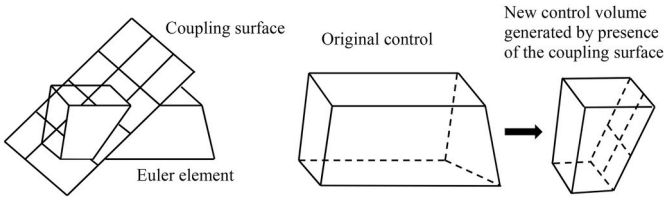

Fig. 7. Schematic diagram of coupling surface and control volume.

more than half of the volume is covered, the adjacent Euler domain will be mixed.

For obtaining accurate results in the simulation of coupling Lagrangian and Eulerian bodies in explicit dynamics, it is necessary to ensure that the size of the cells of the Euler domain are smaller than the minimum distance across the thickness of the Lagrangian bodies. If this is not the case, the leakage of material in the Euler domain through the Lagrange structure would occur, resulting in failure of interaction effect. In the case of coupling to thin bodies, of which the thicknesses are small and typically modelled with shells, an equivalent solid body is generated to enable intersection calculations to be performed between a Lagrangian volume and the Euler domain. The thickness of the equivalent solid body is calculated based on the Euler domain cell size to ensure that at least one Euler element is fully covered over the thickness and no leakage occurs across the coupling surface. It is noted that the 'artificial' thickness is only used for volume intersection calculations for the purposes of coupling and is independent of the physical thickness of the shell/surface body, as shown in Fig. 8. For the shell solver in Autodyn, the parts do not have any geometric through thickness dimension, and as such cannot cover any volume in the Euler mesh. Therefore, each shell part should be artificially thickened. For the coupling methodology to

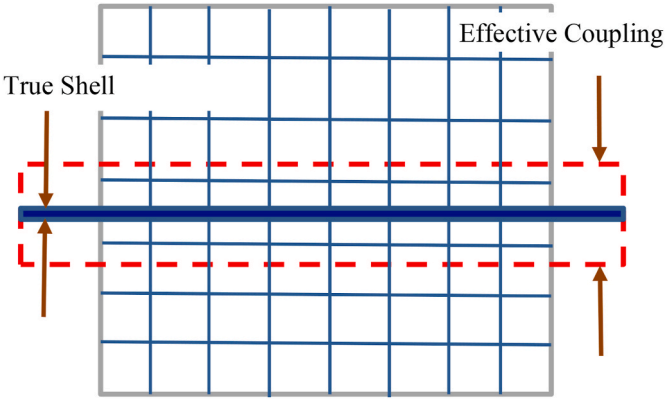

Fig. 8. Schematic diagram of coupling thickness.

function correctly, the artificial thickness of a shell must be at least twice the dimension of the largest cell size in the surrounding Euler grid [39]. In the present numerical simulations, the effective coupling thickness was set to be 25 mm (centred), as the size of the Euler cell is 10 mm.

The shell element was used to model steel plate, the material selected from the library of AUTODYN is 'Piecewise-JC', which allows the definition of a true stress-strain curve as an offset table. Also, Johnson-Cook strain rate dependency can be defined.

$$\frac{\sigma_d}{\sigma_0} = 1 + C\ln(\dot{\varepsilon}^*) \tag{3}$$

where σ_d is the dynamic flow stress corresponding to the dimensionless plastic strain rate $\dot{\varepsilon}^* = \dot{\varepsilon}/\dot{\varepsilon}_0$; $\dot{\varepsilon}$ is the effective plastic strain rate; $\dot{\varepsilon}_0$ is the reference strain rate and chosen to be 1 s^{-1}; σ_0 is the associated static plastic flow stress; C is the empirically determined material constant. This constitutive model is widely used in theoretical and numerical studies on dynamic response of metals under impact and blast loading. For the steel in the present study, $C = 0.22$, and static plastic flow stresses of specimens with different thickness are 360 MPa for 1.6 mm, 317 MPa for 2.3 mm and 343 MPa for 3.7 mm specimens respectively.

Before the simulations were run on the Euler Lagrangian coupling model, the mesh convergence of steel plate was assessed. The aim is to find the influence of different mesh sizes on the accuracy of residual deflection of blast loaded plate and the computational costs. Five conditions of different mesh density of steel plate, including 15 × 15, 20 × 20, 40 × 40, 80 × 80 and 160 × 160 were calculated, and both the dimensionless deflections (divided by the results from 160 × 160 mesh density condition) and dimensionless computation time (divided by the results from 15 × 15 mesh density condition) were compared, as shown in Fig. 9. In the numerical calculations of this paper, the mesh density of 80 × 80 was used guaranteeing a more precise reproduction of the dynamic response of steel plate, while keeping the computational cost low.

Then, the stiffened plates were introduced to the numerical model and the fully Euler-Lagrange coupling is implemented between the steel plates, the wall of blast chamber with venting hole, which was modelled as rigid wall by 8 nodes solid element, and the air inside the confined chamber (just a slice of Euler cell at the horizontal middle cross-section of the whole Euler domain is displayed), as shown in Fig. 10. The blast load was mapped from 2D calculation by using fine mesh. The coupling process of the confined blast pressure and the steel plates with time increasing is shown in Fig. 11. For the sake of clearly showing the interaction effect between Euler cell and Shell/Lagrangian elements, Fig. 11 is displayed in top view of the whole model in Fig. 10. At the beginning of the calculation, the 'artificial' thickness attached to the coupling surfaces was firstly introduced, as shown in Fig. 11 (a). When the steel plates deformed under the confined blast load, the coupling surface moved accordingly to ensure the load applied persistently on the deformed plates. Besides, the deformed plates become updated coupling

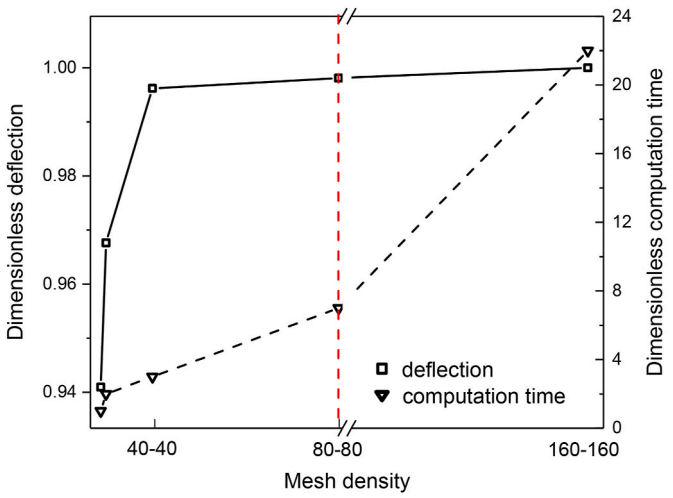

Fig. 9. Relationship between the mesh density and deflection of blast loaded plate and computation time.

interfaces and constrained boundary of Euler cells. In the numerical simulation, no leakage of material in the Euler domain through the steel plate could be found. However, if erosion of the elements of the Lagrangian structure occurs, the coupling interfaces would be automatically updated, and the material in Euler cells would flow through the broken coupling surface.

The dynamic response of 4 samples of stiffened plates are predicted by employing above validated numerical method, and the results of which are compared with experimental data and summarized in Table 1. The numerical results of residual deflections of the central point of stiffened plates agree well with the data from experiments. It is worth noting that the residual deflections in different load conditions from the numerical simulations are the average value of the oscillation stage after the first peak deflections, and those values of experiments were measured by employing a 3D laser scanner after explosion when the plates are in steady condition. Besides, the comparison of the deflection-time histories of a 2.94 mm blast loaded plates (without stiffeners) between numerical simulations and experiments in the conditions of 90 g and 120 g TNT are presented in Fig. 12, which revealed that the numerical method employed in this paper is capable of predicting the dynamic response process of blast loaded plates with acceptable accuracy. The interaction effect between the blast load and the structural response in numerical simulations can also be validated. In the numerical simulations of prototype and small scaled models of blast loaded structures, the above validated mesh density is recommended. Besides, the numerical model can be scaled according to the corresponding geometric scaling factors, but keep the mesh density unchanged.

3. Criteria for altering the stiffener configuration

Rolled and built-up T-type stiffened plates are two of the commonly used strengthening members in large-scale hull structures. Usually, flat bars are often used to replace the T-type stiffeners in small scaled model tests due to manufacturing technical restrictions, in which the configurations of stiffeners are different between prototype and replica. It is essential to guarantee the flat-bar stiffened model to have the similar dynamic characteristics to its T-type stiffened counterpart. Dimensional analysis method is employed to find out the principles that should be followed in altering the stiffener type in the small scaled model of a stiffened plate.

The dynamic response of the blast loaded steel stiffened plate is related to the following parameters, i.e. impulse per unit area of a shockwave I, length of the plate L, thickness of the plate h, material density ρ, number of stiffeners n_0, plastic limit bending moment M_0 and neutral plane force N_0 of stiffeners, dynamic yield stress of material σ_d, cross sectional area of stiffeners S_j, elastic section modulus W_j and moment of inertia I_j.

If take the midpoint deflection w of the stiffened plate as the targeted response, then there is

$$w = f\left(L, h, \rho, M_0, N_0, n_0, I, \sigma_d, S_j, W_j, I_j\right) \tag{4}$$

A set of fundamental dimensions comprised of dynamic yield stress σ_d, material density ρ and length of the plate L are selected to give the following dimensionless π terms.

$$\pi_1 = \frac{h}{L}, \pi_2 = \frac{M_0}{\sigma_d L^3}, \pi_3 = \frac{N_0}{\sigma_d L^2}, \pi_4 = n_0,$$
$$\pi_5 = \frac{I^2}{\sigma_d \rho L^2}, \pi_6 = \frac{S_j}{L^2}, \pi_7 = \frac{W_j}{L^3}, \pi_8 = \frac{I_j}{L^4} \tag{5}$$

The similarity relationship of the dynamic response between the small scaled model and the prototype can be obtained if each term of the

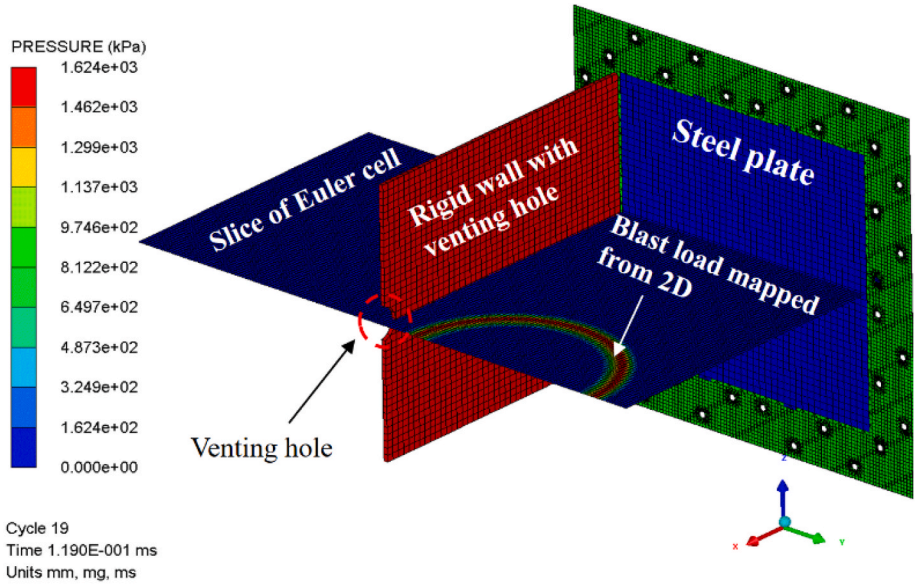

Fig. 10. The numerical model of fully Euler-Lagrange coupling calculation (half model).

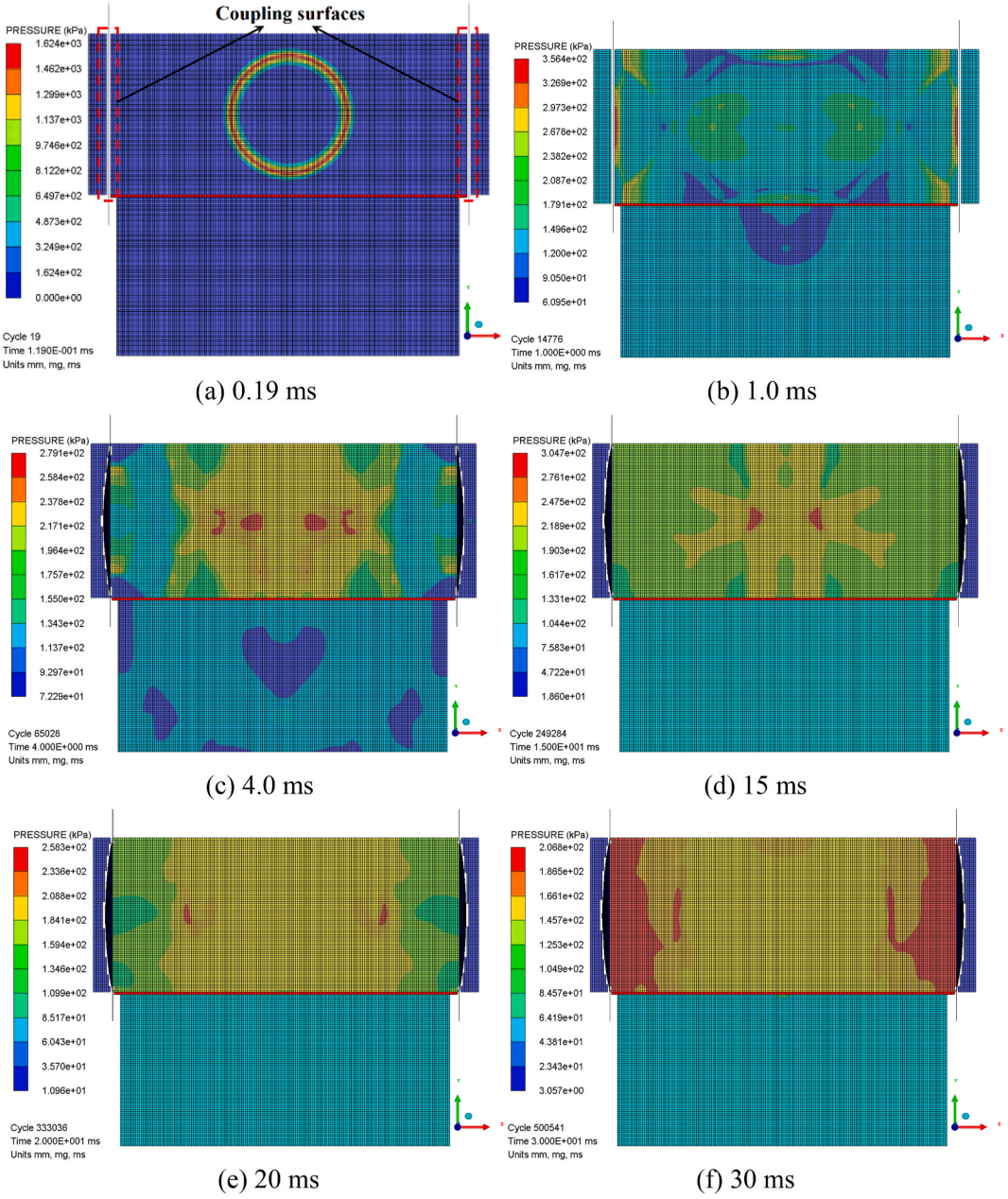

Fig. 11. The movement of coupling surfaces with the deformed steel plates (top view).

Table 1
Results from experimental test and numerical simulations.

No.	TNT mass W (g)	Thickness of plates h (mm)	Stiffener H × W × L (mm)	Number of stiffeners n	Residual deflection of stiffened plates W (mm)	Numerical results (mm)
1	55	1.6	1.6 × 20 × 800	2	35.4	35.2
2	55	2.3	2.3 × 30 × 800	2	26.3	26.4
3	110	2.3	2.3 × 30 × 800	3	43.8	43.7
4	110	3.7	2.7 × 30 × 800	3	24.1	24.0

models is kept equal to their counterparts in the prototype. The geometrical small scaled factor of a stiffened plate is expressed as follows

$$\beta_L^{mp} = L^m / L^p = \beta \tag{6}$$

where L^m and L^p are the length of the small scaled model and prototype, respectively; β is a scaling factor.

The scaled model with complete similarity gives,

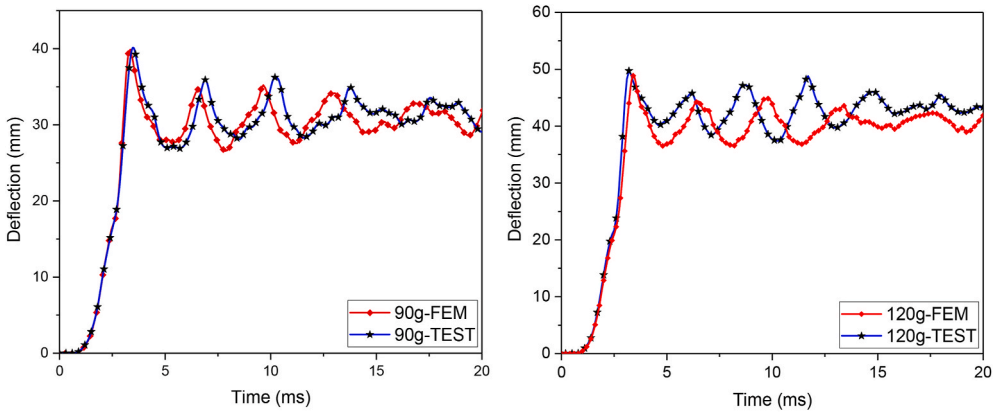

(a) 90 g TNT (b) 120 g TNT

Fig. 12. The comparison of deflection-time histories between numerical simulation and experimental results.

$$\frac{\pi_1^{\mathrm{m}}}{\pi_1^{\mathrm{p}}}=\frac{\beta_h^{\mathrm{mp}}}{\beta_L^{\mathrm{mp}}}=1,\quad \frac{\pi_2^{\mathrm{m}}}{\pi_2^{\mathrm{p}}}=\frac{M_0^{\mathrm{m}}}{M_0^{\mathrm{p}}}\frac{\sigma_{\mathrm{d}}^{\mathrm{p}}}{\sigma_{\mathrm{d}}^{\mathrm{m}}}\left(\frac{L^{\mathrm{p}}}{L^{\mathrm{m}}}\right)^3,\quad \frac{\pi_3^{\mathrm{m}}}{\pi_3^{\mathrm{p}}}=\frac{N_0^{\mathrm{m}}}{N_0^{\mathrm{p}}}\frac{\sigma_{\mathrm{d}}^{\mathrm{p}}}{\sigma_{\mathrm{d}}^{\mathrm{m}}}\left(\frac{L^{\mathrm{p}}}{L^{\mathrm{m}}}\right)^2,\quad \frac{\pi_4^{\mathrm{m}}}{\pi_4^{\mathrm{p}}}=\frac{n_0^{\mathrm{m}}}{n_0^{\mathrm{p}}},$$

$$\frac{\pi_5^{\mathrm{m}}}{\pi_5^{\mathrm{p}}}=\left(\frac{I(t)^{\mathrm{m}}}{I(t)^{\mathrm{p}}}\right)^2\frac{\sigma_{\mathrm{d}}^{\mathrm{p}}}{\sigma_{\mathrm{d}}^{\mathrm{m}}}\frac{\rho^{\mathrm{p}}}{\rho^{\mathrm{m}}}\left(\frac{L^{\mathrm{p}}}{L^{\mathrm{m}}}\right)^2=\frac{(\beta_I^{\mathrm{mp}})^2}{\beta_\sigma\beta^2},\quad \frac{\pi_6^{\mathrm{m}}}{\pi_6^{\mathrm{p}}}=\left(\frac{S_j^m}{S_j^p}\right)\left(\frac{L^{\mathrm{p}}}{L^{\mathrm{m}}}\right)^2,$$

$$\frac{\pi_7^{\mathrm{m}}}{\pi_7^{\mathrm{p}}}=\left(\frac{W_j^m}{W_j^p}\right)\left(\frac{L^{\mathrm{p}}}{L^{\mathrm{m}}}\right)^3,\quad \frac{\pi_8^{\mathrm{m}}}{\pi_8^{\mathrm{p}}}=\left(\frac{I_j^m}{I_j^p}\right)\left(\frac{L^{\mathrm{p}}}{L^{\mathrm{m}}}\right)^4 \tag{7}$$

Among these π terms, π_1, π_4, π_6, π_7 and π_8 are independent variables, while the rest π terms are dependent on the material dynamic properties. The incomplete similarity caused by the strain rate effect was properly corrected by Oshiro and Alves [18]. It should be noted that the values of π_6~π_8 of scaled model might differ from that of the prototype if the configuration (cross-sectional shape) of stiffeners on a stiffened plate is changed due to the restriction of manufacture. Subsequently, other π terms, π_2, π_3 and π_7 in prototype are also unequal to that of the small scaled model. As a result, a dissimilarity occurs in the dynamic response of the prototype and small scaled model. In order to satisfy the requirements of predicting the dynamic behaviour of prototype by using the stiffener-distorted scaled-down models, the terms π_6, π_7 and π_8 need to be identical, which seems impossible. In such the case, therefore, a compromised approach is to keep one or two π terms same, while the others are as close to their counterparts in the ideal small scaled model as possible. Thus, three criteria in scaling the stiffener were considered and compared, i.e.

Criterion 1, keep the cross sectional area of stiffeners S_j the same while make the section modulus W_j and moment of inertia I_j to be as close to their counterparts in the ideal small scaled model as possible.

Criterion 2, keep the section modulus W_j the same while make the cross sectional area of stiffeners S_j and moment of inertia I_j to be as close to their counterparts in the ideal small scaled model as possible.

Criterion 3, keep the moment of inertia I_j the same while make the cross sectional area of stiffeners S_j and the section modulus W_j to be as close to their counterparts in the ideal small scaled model as possible.

Fig. 13 shows the cross sectional dimensions and configurations of T-type and I-type stiffener, respectively.

A square stiffened plate is introduced here to compare the three criteria described above, as shown in Fig. 14. The full-scale stiffened plate is 10 m in length and 10 mm in thickness, with five T cross-section stiffeners (T-type)orthogonally arranged on the plate. The T-type stiffener has dimensions as $\perp\frac{1000\times8}{600\times4}$, which means the length and the thickness of flange are 1000 mm and 8 mm, while the corresponding web sizes are 600 mm and 4 mm, respectively. A blast load was applied on the front side (against the stiffeners) of the plate from an explosion of 1000 kg TNT in 10 m away from the centre of the plate. The numerical simulation is conducted by using ANSYS Autodyn, in which the detailed

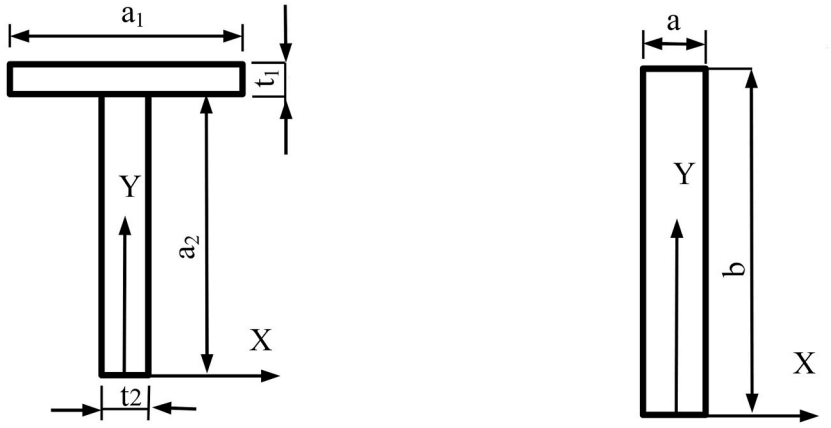

（a）T cross-section stiffener (b) I cross-section stiffener

Fig. 13. Sketch of cross-sections of stiffeners.

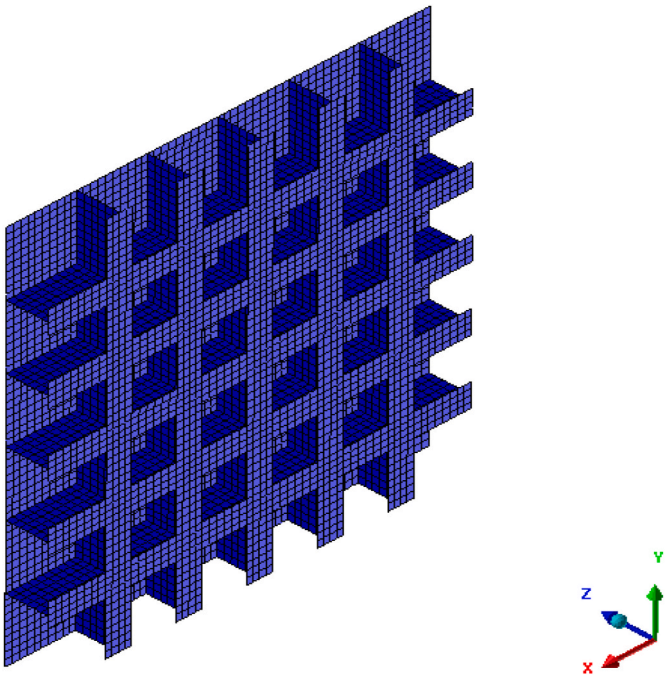

Fig. 14. Schematic diagram of the numerical model of the stiffened panel.

parameters of numerical model are the same with that presented by Zhang et al. [40]. The blast load was directly applied on the front face of stiffened plate by defining the boundary as pressure stress of Analytical Blast in Autodyn [39], in which the propagation of blast wave and its fluid-structure interaction was not taken into consideration in free air explosion. The calculated residual deflection at its centre point of this prototype is 188 mm.

Assuming stiffeners' thickness of small scaled models not to be less than 2 mm, then three kinds of different cross sectional dimensions of the I-shaped stiffeners for the distorted models can be designed according to the above three criteria, which are listed in Table 2. For comparison, a reference model, with both the thickness and configuration of stiffeners being ideally scaled down by a factor of 1:20 from its prototype, is also built to analyse its dynamic behaviour. In this paper, the 1:20 scaling problem was solved by employing equations and numerical simulation to illustrate the application process of the present method. Actually, any other scaling factor can be used. However, an appropriate scaling factor between prototype and small scaled model should be determined due to some restrictions in practice. It should be noted that the numerical model of the small scaled structure has the same amount of grids with the prototype model.

Selecting the dynamic response of the plates at the centre point of the stiffened plate as an object, the comparison results of deflection and velocity-time curves for each small scaled model in complying with the related three criteria are shown in Figs. 15 and 16. The comparative results show that the plate designed conforming to Criterion 2 has the most similar behaviour with the ideal reference model no matter in displacement or velocity under blast loads. This indicates that the stiffeners may have reasonably approximate dynamic behaviour when keep the section modulus the same while make the other two terms to be as close to their counterparts as possible. Based on the analysis above, Criterion 2 for stiffeners will be employed in the following analysis. The small scaled model designed by employing the Criterion 1, which had the same cross section area with the reference model, experienced much larger deflection. It means that it is the absorption of the bending energy but not the inertial effect of the stiffeners mainly affected the dynamic behaviour of the blast loaded stiffened plates.

Although Criterion 2 ensures the stiffened plate with distorted stiffener having the most similar dynamic behaviour to its prototype, it should be noted that the dynamic response of the stiffener distorted model still has deviations from that of the reference model. It needs further corrections before it can be used to predict the dynamic response of its prototype, in which the schematic diagram for altering the configuration of stiffener is shown in Fig. 17. A distorted geometric parameter of the stiffener could be taken into account to help building a more accurate similarity relation between the stiffener distorted small scaled mode and the prototype.

Considering the overall deflection of the stiffened plate to be closely related to its energy absorption, the energy absorption of stiffeners (as a part of the stiffened plate) will be affected by their plastic limit bending moment M_0 and neutral plane force N_0. The cross sectional area S_j of the stiffeners may be selected as the geometrical correction parameter.

The plastic limit bending moment M_0 of stiffeners can be obtained from the following formula,

$$M_0 = \sigma_d(S_1 + S_2) = 0.5\sigma_d S_j(l_1 + l_2) \tag{8}$$

The neutral plane force N_0 of stiffeners corresponding to plastic limit is,

$$N_0 = \sigma_d S_j \tag{9}$$

where S_1 and S_2 are the static moments from the compression and tension areas to the neutral axis of the cross-sectional area of the stiffener, respectively; l_1 and l_2 represent the distance from the centroid of the compression and tension area to the neutral axis of the cross-sectional area of the stiffener, respectively.

A geometrical distortion factor about the cross sectional area S_j of the stiffener is defined as follows,

Table 2
Cross sectional parameters of the small scaled stiffeners.

Criterion No.	Reference model (stiffeners are ideally scaled down)	1	2	3
Cross sectional dimension (mm)	$\perp\frac{50\times0.4}{30\times0.5}$	18×2	41×2	43×2
Cross sectional area S_j (mm^2)	35	36	82	86
Section modulus W_j (mm^3)	1080	216	1121	1233
moment of inertia I_j(mm^4)	54542	3888	45947	53005
TNT mass W (kg)	0.125	0.125	0.125	0.125
Stand-off distance R (mm)	500	500	500	500

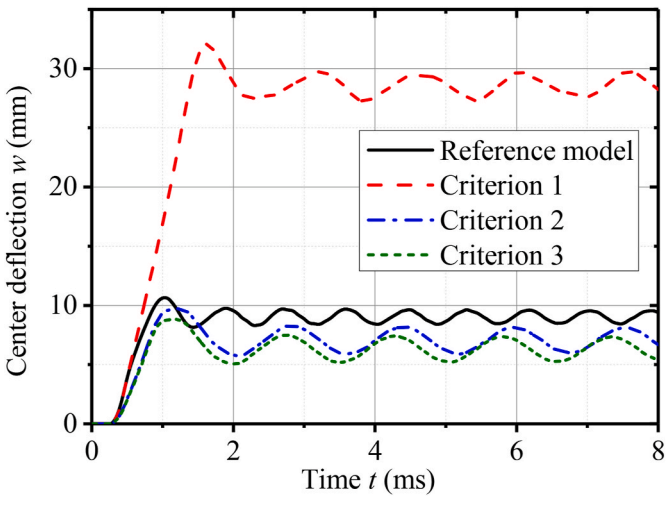

Fig. 15. Comparison of the deflection-time curves among the three criteria.

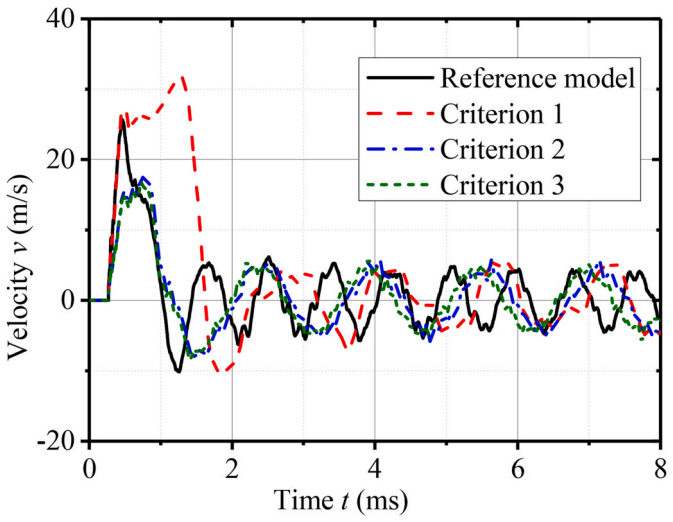

Fig. 16. Comparison of the velocity-time curves among the three criteria.

$$\beta_{S_j} = (S_j)^d / (S_j)^p \tag{10}$$

where $(S_j)^d$ and $(S_j)^p$ represent the cross sectional areas of distorted small scaled stiffener and prototype stiffener, respectively.

Besides, a corresponding distortion coefficient of the cross sectional area is defined below,

$$\lambda_{S_j} = (S_j)^d / (S_j)^m = \beta_{S_j} / \beta \tag{11}$$

Thus a correction equation for the impulse per unit area of the shockwave I^c is given by

$$I^c = I^m \lambda_I = I^m \lambda_{S_j}{}^{n_I} \tag{12}$$

where I^m and I^c are the impulse per unit area applied on the reference model and the distorted model, respectively. n_I is an exponent related to the distorted geometrical parameters and the impulse per unit area.

The corrected TNT mass for the distorted model can be determined based on the result of Eq. (12), of which the flow chart is shown in Fig. 18. Firstly, a pair of small scaled models with different distortion scaling factors of the cross section, Model A and Model B were designed and introduced. The detailed parameters of the three different models of the stiffener plates are listed in Table 3, in which the reference model is the ideally scaled model with no distortion parameters.

By employing the verified numerical method presented in Section 1, a series of numerical calculations with different loading conditions of TNT mass were performed to predict the dynamic response of the three small scaled models, as listed in Table 4.

A set of data of the centre point deflection (w) and the impulse per unit area (I) for each model are collected, and their relationship (I-w curve) can be determined subsequently by data fitting. Thus two I-w relationships F_1 and F_2 for Model-A and Model-B can be established, which are given as

$$F_1 : w_A = 0.0555 I_A - 12.863 \tag{13}$$

$$F_2 : w_B = 0.0533 I_B - 12.308 \tag{14}$$

The fitting relationship for TNT mass and impulse per unit area (W-I curve) from the numerical simulations is given as

$$W = 0.6321 I - 101.02 \tag{15}$$

For example, when the load from the explosion of 125 g TNT was applied to the reference model, as listed in Table 3, the value of the impulse per unit area I^m applied on the stiffened plate was calculated by Eq. (15), $I^m = 357 Pa{\cdot}s$. The correction exponent n_I can be solved by taking I^m, F_1 and F_2 into the computing programs, with its value determined as 0.112. Thus the corrected impulse per unit area for Model-A is

$$I_A{}^c = I^m \lambda_{SA}{}^{n_I} = 357 \times 2.34^{0.112} = 392 \ \text{Pa·s} \tag{16}$$

The corresponding corrected TNT mass for Model-A is 147 g, which can be acquired by inserting the value of $I_A{}^c$ in Eq. (15). By applying the corrected TNT mass to the Model-A (here the Model-A is employed to predict the dynamic response of the prototype), a value of 8.91 mm in residual centre deflection of the stiffened plate is obtained, which is very close to that of the reference model (8.92 mm). Here, the residual centre deflection of the model is the average value of crest and trough in the

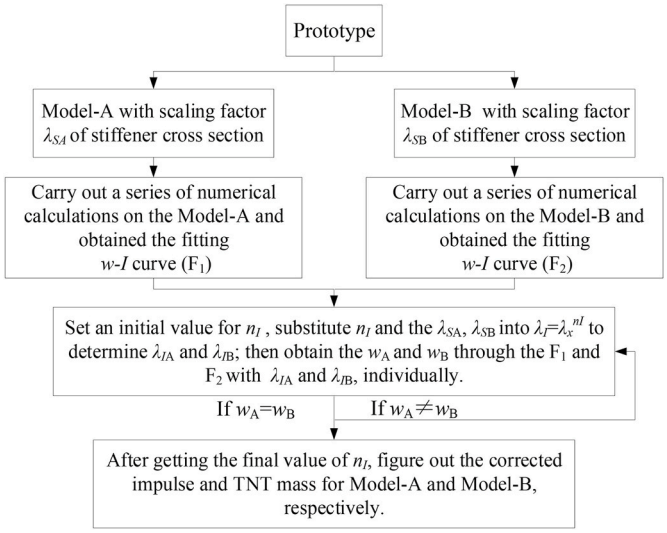

Fig. 18. The flow chart of the method for determining the corrected TNT mass.

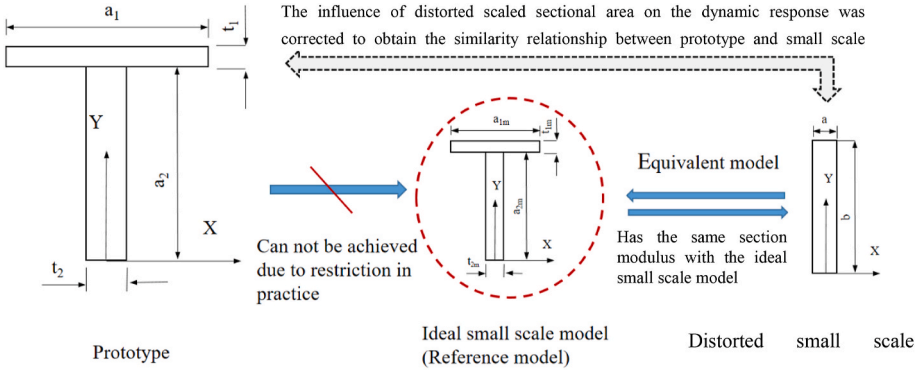

Fig. 17. The schematic diagram for altering the configuration of stiffener.

Table 3
Relevant parameters of the two stiffener-distorted models.

Name	Stiffener (mm)	Cross section S_j (mm^2)	Section modulus W_j (mm^3)	Moment of inertia I_j (mm^4)	Distortion coefficient of the cross section λ_{Sj}
Reference model	$\frac{50 \times 0.4}{\perp 30 \times 0.5}$	35	1080	54543	1.00
Model-A	41 × 2	82	1121	45947	2.34
Model-B	36 × 2.5	90	1080	38880	2.57

Table 4
The computing results of each distorted model.

No.	Model-A1	Model-A2	Model-A3	Model-A4	Model-A5	Model-A6
TNT mass (g)	130	135	140	145	150	155
I (Pa·s/m^2)	365.07	373.29	381.38	389.35	397.20	404.93
w (mm)	7.39	7.86	8.32	8.75	9.20	9.61
No.	Model-B1	Model-B2	Model-B3	Model-B4	Model-B5	Model-B6
TNT mass (g)	170	175	180	185	190	195
I (Pa·s/m^2)	427.49	434.81	442.04	449.17	456.22	463.18
w (mm)	1045	10.82	11.26	12.65	12.01	12.38

oscillation stage of the curve. The comparison of deflection- and velocity-time predictive curves between the reference model and Model-A with the corrected TNT mass are shown in Figs. 19 and 20, respectively.

As indicated in Fig. 18, the difference of residual centre deflection between the corrected model and the reference model is relatively small, though there is a deviation in their maximum displacement. Although the predicted maximum velocity (Fig. 20) is not as good as the deflection in comparison to that of the reference model, the overall velocity-time history curve predicted has better correlation than the results in Fig. 16. These comparison results indicate that the influence of the change of the cross sectional area S_j of the small scaled model on the similarity of the dynamic behaviour between replica and prototype can be effectively corrected by using the updated TNT mass.

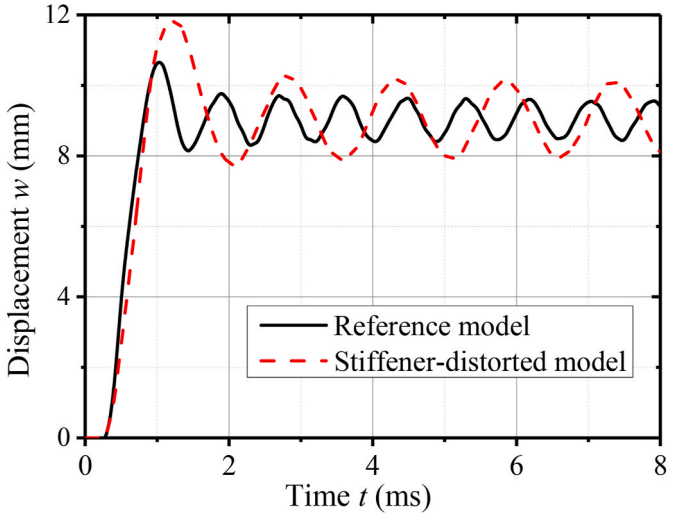

Fig. 19. Comparison of the displacement-time histories between the stiffeners distorted model and the reference model.

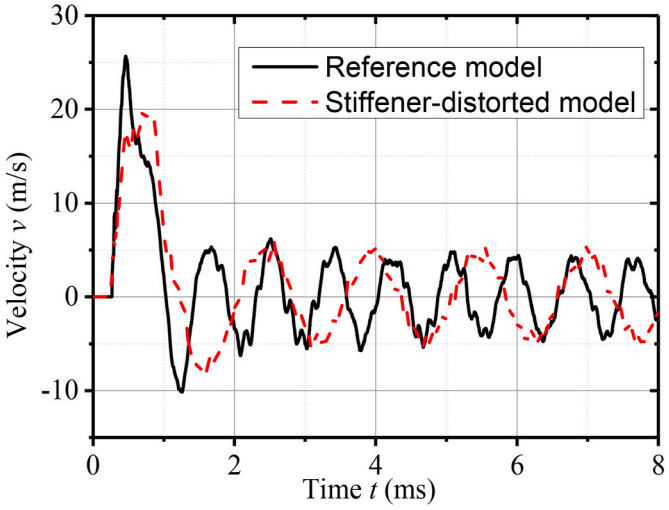

Fig. 20. Comparison of the velocity-time histories between the stiffeners distorted model and the reference model.

4. Scaled models considering double geometric parameters

In this section a more complex situation of the distorted small scaled model in both stiffener types and thickness of the plate will be further studied based on the corrected method for stiffener distorted model presented in Section 3.

For the models distorted in both stiffener configuration and thickness of plates, the correction equation Eq. (12) used in the stiffener distorted model can be developed into the following form

$$I^{c} = I^{m}(\lambda_h)^{n_{I1}} \left(\lambda_{S_j}\right)^{n_{I2}} \tag{17}$$

where n_{I1} and n_{I2} are two exponents related to the distorted scaling thickness of plates and the cross sectional area of stiffeners, respectively.

The difficulty in using Eq. (17) to obtain a correct factor of I^c is how to determine the value of the first coefficient n_{I1} for a scaled model considering double geometric parameters double geometric parameter distorted model and thus pose a barrier to solve the second unknown exponent $n_{I2}$with the method proposed in our previous research work [35].

In order to solve the exponents in Eq. (17), it is necessary to simplify this equation. Considering the exponent n_x has a fixed value in a specific distorted model, if the thickness of the plate of this model is distorted with a fixed distortion coefficient λ_h, then the item $(\lambda_h)^{n_{I1}}$ in Eq. (17) can be replaced with an unknown constant C and thus

$$I^{c} = I^{m} C \left(\lambda_{S_j}\right)^{n_{I2}} \tag{18}$$

Here, the simplified Eq. (18) can be solved according to the following steps.

Step 1: establish three distorted models Model-A, Model-B and Model-C with identical size, which have the same plate thickness to ensure the same thickness distortion coefficients λ_h but with different cross sectional area and stiffeners distortion coefficients, i.e. λ_{SA}, λ_{SB} and λ_{SC}. It should be noted that the distorted small scaled model in cross sectional area of stiffeners should follow Criterion 2 given in Section 2. Then a series of TNT mass selected from a narrow range deviated from the TNT mass W^m of the small scaled reference model (without distortion) are applied to the distorted models to calculate the dynamic response numerically.

Step 2: take one parameter of dynamic response as the object of study, for instance, the deflection w of the plates. Then the relation between corrected I^c and deflection of each small scaled model can be given as follows,

$$\begin{aligned} \mathrm{F_A}: w = g_A\left(I_A{}^c\right) &= g\left(I^m C\lambda_{S_A}{}^{n_{I2}}\right) \\ \mathrm{F_B}: w = g_B\left(I_B{}^c\right) &= g\left(I^m C\lambda_{S_B}{}^{n_{I2}}\right) \\ \mathrm{F_C}: w = g_C\left(I_C{}^c\right) &= g\left(I^m C\lambda_{S_C}{}^{n_{I2}}\right) \end{aligned} \tag{19}$$

Step 3: employ Newton method to solve the above equation set and the values of w, C and n_{I2} can then be determined. Also, n_{I1} is obtained from $C = (\lambda_h)^{n_{I1}}$.

The above steps can be implemented by programming. After determining the value of n_{I1} and n_{I2}, the corrected value of impulse per unit area for the distorted small scaled model with double geometric parameters can be computed. Subsequently the corrected TNT mass for the distorted model can also be determined. Furthermore, by applying the corrected TNT mass to the distorted model, the similar dynamic behaviour can be evaluated between the distortedly small scaled model and the prototype.

5. Scaling the dynamic behaviour of blast loaded structure

5.1. The dynamic behaviour of a stiffened plate under free air blast load

The typical stiffened plate studied in Section 3 was employed to verify the method of the distorted small scaled models with double geometric parameters proposed in Section 3. Here, three sets of the distorted models, Model-A, Model-B and Model-C, are established to calculate values of n_{I1} and n_{I2}. The relevant parameters are summarized in Table 5.

A series of TNT mass W of 190, 195, 200, 205 and 210 g are selected and the values of their corresponding impulse per unit area of the shockwave I applied on the stiffened plate are computed. The W-I fitting formula is given as follows,

$$W = 0.7314I - 143.73 \tag{20}$$

By applying the above TNT masses selected to the distorted models, the final deflection at the centre point of blast loaded stiffened plates can be obtained. Then a set of w-I formulas can be fitted and given as follows,

$$\begin{aligned} &\text{Model}-\text{A}, \quad \mathrm{F_A}: w_A = 0.0445I_A - 10.998 \\ &\text{Model}-\text{B}, \quad \mathrm{F_B}: w_B = 0.0432I_B - 10.811 \\ &\text{Model}-\text{C}, \quad \mathrm{F_C}: w_C = 0.0549I_C - 14.804 \end{aligned} \tag{21}$$

For the 1:20 ideal small scaled reference model, its TNT mass W^{m} is 127.5 g after taking the scaling factor and strain-rate effect into account and the value of the corresponding impulse per unit area I_0 of the adjusted TNT mass is 359 Pa·s. Substituting the I_0 determined into Eq. (19), the values of C and n_{I2} are obtained as below.

$$C = 1.02, \quad n_{I2} = 0.216 \tag{22}$$

The corrected impulse $I_A{}^c$ of Model-A stiffener plate at the centre point is $I_A{}^c = 440.1$ *Pa·s* and finally, the corrected TNT mass $W_A{}^c$ for Model-A is obtained by Eq. (20) as 178.2 g.

By applying the updated TNT mass to Model-A, the residual deflection 8.60 mm of the stiffener plate at its centre point can be obtained through numerical calculations. Based on the result of Model-A, the corresponding value of the residual defection of the prototype predicted is 172 mm, which is very close to the value of 188 mm calculated directly from the full-size structure. Figs. 21 and 22 show the comparison of the predicted displacement- and velocity-time history curves from the uncorrected model, the corrected distorted model and the prototype, respectively. It is found that the present corrected method provides a better prediction of the dynamic behaviour of the full-size structure, reducing the deviation from 47% to 8.48%, as shown in Fig. 21. It is worth noting that the TNT mass for the uncorrected model was determined according to the geometrical scaling factor, which is approximately equal to the cube root of the TNT mass for the prototype. That is to say, the influence of the distortion scaling factors on the dynamic response was not considered for the uncorrected model, resulting in much lower predicted deflection than that of the corrected model when subjected to blast load. Although the predicted velocity shows some discrepancy, the corrected model still gives better predicted results of the maximum velocity for the prototype, as shown in Fig. 22.

5.2. The dynamic behaviour of a stiffened plate subjected to confined blast load

Take the four stiffened plates listed in Table 1 as prototypes, three distorted small scaled models with double geometric parameters for each prototype were designed to determine the value of C and n_{I2} by employing the method presented in Section 4. The relevant geometric parameters of each distorted small scaled model are given in Table 6.

Here taking Case No.1 as an example to predict its dynamic behav-

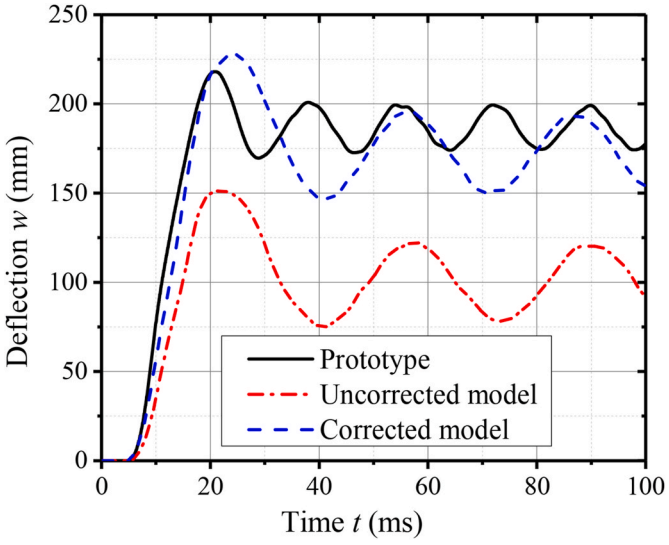

Fig. 21. Comparison of the deflection-time histories between prototype, uncorrected and corrected models.

Table 5
Detailed parameters of each distorted model.

Name	Scaling factor β	Length l (mm)	Thickness h (mm)	Thickness distortion coefficient λ_h	Stiffener (mm)	Cross Sectional area S_j (mm^2)	Cross Sectional area distortion coefficient λ_{sj}
Prototype	1.0	10000	10	1.0	$\perp\frac{1000\times 8}{600\times 10}$	14000	1.0
Scale-down reference model	0.05	500	0.5	1.0	$\perp\frac{50\times 0.4}{30\times 0.5}$	35	1.0
Model-A	0.05	500	1.0	2.0	41 × 2.0	82	2.34
Model-B	0.05	500	1.0	2.0	36 × 2.5	90	2.57
Model-C	0.05	500	1.0	2.0	47 × 1.5	70.5	2.01

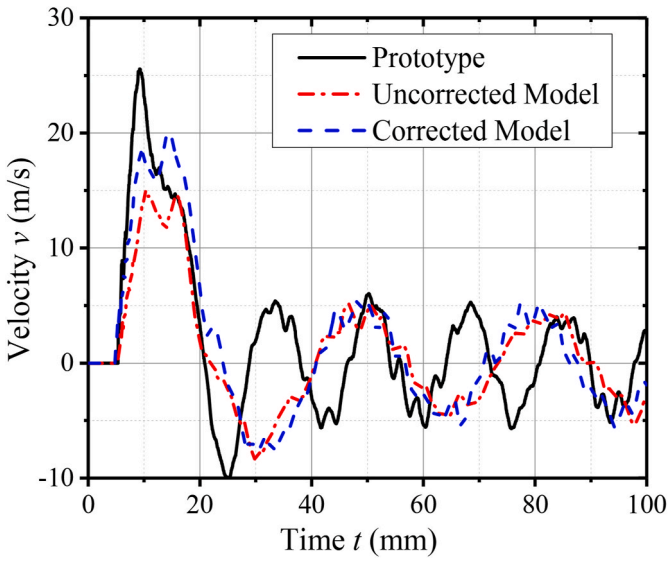

Fig. 22. Comparison of the velocity-time histories between prototype, uncorrected and corrected models.

iour under confined blast load by using three 1:10 small scaled models, both the geometric parameter of plate thickness and the size of stiffener are distorted small scaled with different factors. It is noted that the design of distorted stiffeners follows Criterion 2 presented in Section 2, which keeps the section modulus W_j unchanged, while the cross sectional area of stiffenersS_j and moment of inertia I_j are as close to their counterparts of the ideal small scaled model as possible. The detailed parameters of the scaled stiffener in Case No.1 are listed in Table 7.

A series of TNT masses, which are close to the mass ideally scaled down by using the overall scaling factor are applied to Model-A, Model-B and Model-C and the corresponding residual deflection at the centre point of the stiffeners plates are collected. The validated numerical method was employed to conduct the dynamic responses of different models under the confined blast load from different masses of TNT. With the data collected three sets of the *w-I* equation for each model are obtained, which are given as follows,

$$\begin{aligned} &\text{Model}-\text{A},\ \ \text{F}_\text{A}: w_A = 0.2364 I_A + 0.2945 \\ &\text{Model}-\text{B},\ \ \text{F}_\text{B}: w_B = 0.2186 I_B + 0.5255 \\ &\text{Model}-\text{C},\ \ \text{F}_\text{C}: w_C = 0.2661 I_C - 0.1944 \end{aligned} \tag{23}$$

and so as the *W-I* relation,

$$W = 1.044 \times 10^{-2} I - 9.524 \times 10^{-3} \tag{24}$$

The TNT mass W for the prototype is 55 g, thus the TNT mass W^m applied to the 1:10 ideal small scaled model (without geometric distortion) needs to be determined. The corresponding impulse per unit area I^m at the centre point of the ideal small scaled stiffener plate is 6.054 Pa·s. Solving Eq. (23) with the above parameters, the values of C and n_{I2} are obtained.

$$C = 2.349, \quad n_{I2} = 0.073 \tag{25}$$

Then, the corrected value of the impulse per unit area $I_A{}^c$ for Model-A is 14.343 Pa·s and a corrected TNT mass is determined from Eq. (24). The updated TNT mass is then applied in the numerical simulations by the distorted small scaled model. The comparison of the displacement- and velocity-time history curves of the prototype, the predicted value from uncorrected and corrected models are shown in Figs. 23 and 24, respectively. It is found that a good agreement is achieved, of which the value of residual deflection of the prototype stiffened plate predicted by the corrected Model-A is 36.9 mm, while that from the experimental test and numerical simulation of the full size stiffened plate given in Table 1 are 35.4 mm and 35.2 mm. The errors on the predicted residual deflections are 4.02% and 4.63%, respectively. It is obvious that the predicted deflection by using uncorrected model is much lower than that of the prototype and corrected model, for the uncorrected TNT mass was employed in the numerical simulations, while the TNT mass applied to the corrected model was properly altered according to the double distortion scaling factors of the stiffened plate by employing the method presented in this paper.

The dynamic responses predicted for rest of the cases with the same correction method are listed in Table 8. Clearly, the corrected method proposed in this paper is capable of determining the dynamic behaviour of the full size stiffened plate by using the double geometric distortedly small scaled model with an acceptable accuracy.

Table 6
Geometric parameters and scaling factor of each distorted small scaled model.

No.	Scaling factor β	Distortion coefficient of the thickness of plates λ_h	Cross sectional area of stiffeners (mm)		
			Model-A	Model-B	Model-C
1	0.1	2	1.8 × 0.2	1.6 × 0.25	1.5 × 0.3
2	0.1	2	2.9 × 0.25	2.6 × 0.3	2.4 × 0.35
3	0.1	2	2.9 × 0.25	2.6 × 0.3	2.4 × 0.35
4	0.1	2	2.8 × 0.3	2.6 × 0.35	2.5 × 0.4

6. Conclusions

A verified numerical method in calculating the confined blast load and dynamic response of stiffened plate was presented. By employing remapping technique, the pressure distribution of blast load in a 2D domain could be mapped into a 3D domain with higher accuracy comparing to that directly obtained from the 3D calculation. The predicted results from the numerical method presented in this paper agree well with the experimental data both in confined blast and deflection of stiffened plate. Based on the Hopkinson scaling law, the numerical method can be further employed to predict the blast load and dynamic response of small scaled model and prototype of structures, which provides a reliable means to verify the proposed similarity method.

A corrected scaling method for predicting the dynamic behaviour of the prototype of stiffened plates under blast loads by using its distortedly small scaled model with double-geometric parameters has been proposed and verified in this paper. The situations of both the thickness of the plate and the type of stiffeners are distortedly small scaled with different factors are considered. Unlike the single-geometric parameter distorted case, the double-geometric parameters distortedly small scaled model has to be more carefully designed and the distortion of their stiffeners should conform to Criterion 2 outlined in Section 3. It is worth noting that the section modulus of the stiffener should be given priority to distorting the stiffener configuration, the cross sectional area and the moment of inertia of the stiffener, as close to that of the ideal small scaled model as possible. This is the key point to keep the stiffener distortedly small scaled model having the most similar dynamic behaviour to its prototype. It also guarantees that the present correction method will be smoothly employed in predicting the dynamic response of the prototype stiffened plates by using the well-designed distorted model.

The present study would provide a potential approach to deal with the multi-geometric parameters distorted stiffener plate. However, it is better to reduce the number of the distorted geometric parameters (within the experimental restrictions) as small as possible to make sure a

Table 7
Parameters of the stiffeners in Case No.1

Case No.1	Scaling factor β	Stiffener (mm)	Cross sectional area S_j (mm^2)	Section modulus W_j (mm^3)	Moment of inertia I_j (mm^4)	Distortion coefficient of cross section area λ_{sj}
Prototype	1	20 × 1.60	32	213	4267	1.000
Model-A	0.1	1.8 × 0.20	0.36	0.216	0.3888	1.125
Model-B	0.1	1.6 × 0.25	0.40	0.213	0.3413	1.250
Model-C	0.1	1.5 × 0.3	0.45	0.225	0.3375	1.406

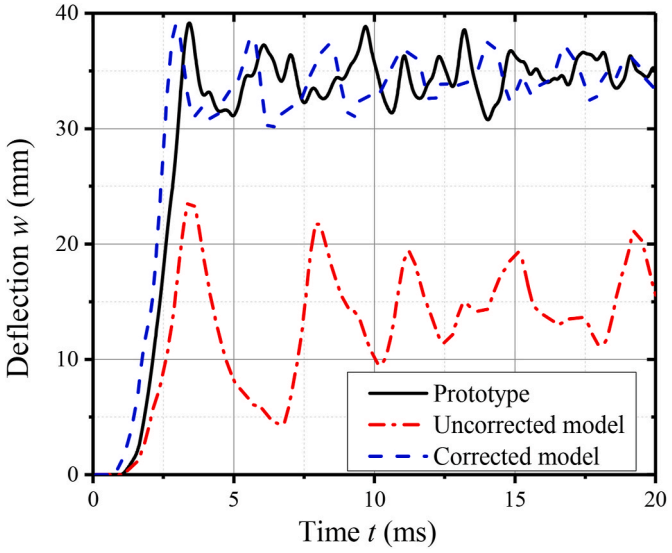

Fig. 23. Predicted deflection-time curves of the uncorrected and corrected models.

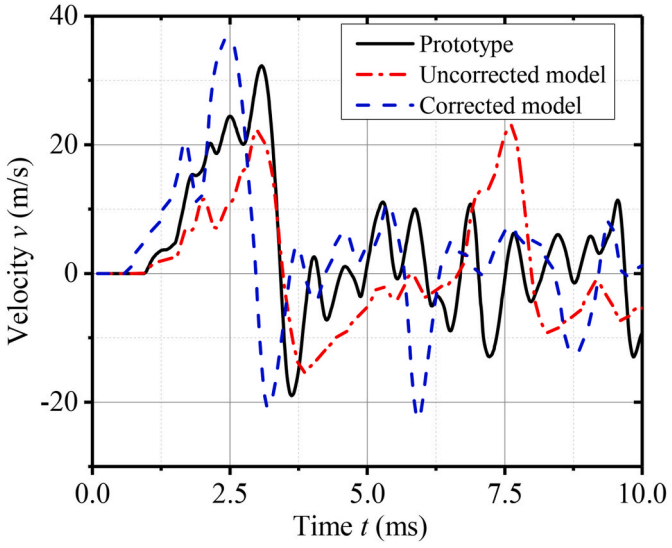

Fig. 24. Predicted velocity-time curves of the uncorrected and corrected models.

most similar dynamic response to be obtained between the distorted model and the prototype. In addition, the different mechanical parameters of plates with different thicknesses would be considered in practice test, which was not taken into account in the numerical simulations in present paper.

Table 8
Predicted results of the double-parameter distorted model in each case.

Case No.	1	2	3	4
TNT mass W (g)	0.055	0.055	0.011	0.011
Stand-off distance R (mm)	90	90	90	90
Scaling factor β	0.1	0.1	0.1	0.1
Distortion coefficient of the thickness of plates λ_h	2.0	2.0	2.0	2.0
Stiffener of the small scaled distorted model (mm)	1.8 × 0.2	2.9 × 0.25	2.9 × 0.25	2.8 × 0.3
Constant C	2.349	2.973	2.257	2.695
Correction exponent n_I	0.073	0.037	−0.014	0.010
Corrected impulse per unit area I (Pa·s)	14.343	18.03	25.78	30.843
Corrected TNT mass $W(g)$	0.140	0.178	0.262	0.316
Numerical results of the center deflection w^c (mm)	3.465	2.800	4.512	2.421
Prediction result w^p (mm)	34.65	28.00	45.12	24.21
Error (%)	2.14	6.22	3.18	0.75

Author statement

All persons who have made substantial contributions to the work reported in the manuscript, including those who provided editing and writing assistance but who are not authors, are named in the Acknowledgments section of the manuscript and have given their written permission to be named.

Declaration of competing interest

The authors declare that they have no known competing financial interests or personal relationships that could have appeared to influence the work reported in this paper.

Acknowledgements

The authors acknowledge Projects supported by the Joint Foundation for Young Scientists of Ministry of Education (6141A02033108) and National Natural Science Foundation of China (11502180). The authors are also grateful for the valuable suggestions from Professor Magnus Langseth.

References

[1] M.A.G. Calle, M. Alves, A review-analysis on material failure modeling in ship collision, Ocean Eng. 106 (2015) 20–38.
[2] X.S. Kong, W.G. Wu, J. Li, P. Chen, F. Liu, Experimental and numerical investigation on a multi-layer protective structure under the synergistic effect of blast and fragment loadings, Int. J. Impact Eng. 65 (2014) 146–162.
[3] K. Micallef, A.S. Fallah, D.J. Pope, L.A. Louca, The dynamic performance of simply-supported rigid-plastic circular steel plates subjected to localised blast loading, Int. J. Mech. Sci. 65 (1) (2012) 177–191.
[4] R.G. Teeling-Smith, G.N. Nurick, The deformation and tearing of thin circular plates subjected to impulsive loads, Int. J. Impact Eng. 11 (1) (1991) 77–91.
[5] N. Jacob, G.N. Nurick, G.S. Langdon, The effect of stand-off distance on the failure of fully clamped circular mild steel plates subjected to blast loads, Eng. Struct. 29 (10) (2007) 2723–2736.
[6] N. Mehreganian, A.S. Fallah, L.A. Louca, Inelastic dynamic response of square membranes subjected to localised blast loading, Int. J. Mech. Sci. 148 (2018) 578–595.

[7] C. Zheng, X.-s. Kong, W.-g. Wu, F. Liu, The elastic-plastic dynamic response of stiffened plates under confined blast load, Int. J. Impact Eng. 95 (2016) 141–153.
[8] K. Micallef, A.S. Fallah, P.T. Curtis, L.A. Louca, On the dynamic plastic response of steel membranes subjected to localised blast loading, Int. J. Impact Eng. 89 (2016) 25–37.
[9] J. Zhang, Q. Qin, T.J. Wang, Compressive strengths and dynamic response of corrugated metal sandwich plates with unfilled and foam-filled sinusoidal plate cores, Acta Mech. 224 (4) (2013) 759–775.
[10] J. Zhang, R. Zhou, M. Wang, Q. Qin, Y. Ye, T.J. Wang, Dynamic response of double-layer rectangular sandwich plates with metal foam cores subjected to blast loading, Int. J. Impact Eng. 122 (2018) 265–275.
[11] X. Cui, L. Zhao, Z. Wang, H. Zhao, D. Fang, Dynamic response of metallic lattice sandwich structures to impulsive loading, Int. J. Impact Eng. 43 (2012) 1–5.
[12] C.P. Coutinho, A.J. Baptista, J. Dias Rodriges, Modular approach to structural similitude, Int. J. Mech. Sci. 135 (2018) 294–312.
[13] A. Neuberger, S. Peles, D. Rittel, Scaling the response of circular plates subjected to large and close-range spherical explosions. Part I: air-blast loading, Int. J. Impact Eng. 34 (5) (2007) 859–873.
[14] A. Neuberger, S. Peles, D. Rittel, Scaling the response of circular plates subjected to large and close-range spherical explosions. Part II: buried charges, Int. J. Impact Eng. 34 (5) (2007) 874–882.
[15] X. Zhao, V. Tiwari, M.A. Sutton, X. Deng, W.L. Fourney, U. Leiste, Scaling of the deformation histories for clamped circular plates subjected to blast loading by buried charges, Int. J. Impact Eng. 54 (2013) 31–50 (0).
[16] L.F. Trimiño, D.S. Cronin, Non-direct similitude technique applied to the dynamic axial impact of bonded crush tubes, Int. J. Impact Eng. 64 (2014) 39–52.
[17] M.A.G. Calle, R.E. Oshiro, M. Alves, Ship collision and grounding: scaled experiments and numerical analysis, Int. J. Impact Eng. 103 (2017) 195–210.
[18] R.E. Oshiro, M. Alves, Scaling of structures subject to impact loads when using a power law constitutive equation, Int. J. Solid Struct. 46 (18–19) (2009) 3412–3421.
[19] R.E. Oshiro, M. Alves, Predicting the behaviour of structures under impact loads using geometrically distorted scaled models, J. Mech. Phys. Solid. 60 (7) (2012) 1330–1349.
[20] G.K. Schleyer, S.S. Hsu, M.D. White, Scaling of pulse loaded mild steel plates with different edge restraint, Int. J. Mech. Sci. 46 (9) (2004) 1267–1287.
[21] I.M. Snyman, Impulsive loading events and similarity scaling, Eng. Struct. 32 (3) (2010) 886–896.
[22] W. Wang, D. Zhang, F. Lu, S.-C. Wang, F. Tang, Experimental study on scaling the explosion resistance of a one-way square reinforced concrete slab under a close-in blast loading, Int. J. Impact Eng. 49 (2012) 158–164 (0).
[23] H.-M. Wen, N. Jones, Experimental investigation of the scaling laws for metal plates struck by large masses, Int. J. Impact Eng. 13 (3) (1993) 485–505.
[24] F.J. Yang, M.Z. Hassan, W.J. Cantwell, N. Jones, Scaling effects in the low velocity impact response of sandwich structures, Compos. Struct. 99 (2013) 97–104 (0).
[25] T. Noam, M. Dolinski, D. Rittel, Scaling dynamic failure: a numerical study, Int. J. Impact Eng. 69 (2014) 69–79.
[26] N. Jones, Structural Impact, Cambridge University Press, Cambridge, 1997.
[27] A. Morquio, J.D. Riera, Size and strain rate effects in steel structures, Eng. Struct. 26 (5) (2004) 669–679.
[28] R.E. Oshiro, M. Alves, Scaling impacted structures, Arch. Appl. Mech. 74 (1–2) (2004) 130–145.
[29] R.E. Oshiro, M. Alves, Scaling of cylindrical shells under axial impact, Int. J. Impact Eng. 34 (1) (2007) 89–103.
[30] L.M. Mazzariol, R.E. Oshiro, M. Alves, A method to represent impacted structures using scaled models made of different materials, Int. J. Impact Eng. 90 (2016) 81–94.
[31] Z. Luo, Y. Zhu, X. Zhao, D. Wang, Determination method of dynamic distorted scaling laws and applicable structure size intervals of a rotating thin-wall short cylindrical shell, Proc. IME C J. Mech. Eng. Sci. 229 (5) (2015) 806–817.
[32] Z. Luo, Y.P. Zhu, X.Y. Zhao, D.Y. Wang, High-order vibrations' dynamic scaling laws of distorted scaled models of thin-walled short cylindrical shells, Mech. Base. Des. Struct. Mach. 43 (4) (2015) 514–534.
[33] U. Cho, A.J. Dutson, K.L. Wood, R.H. Crawford, An advanced method to correlate scale models with distorted configurations, J. Mech. Des. 127 (1) (2005) 78–85.
[34] S. Yao, D. Zhang, F. Lu, X. Chen, P. Zhao, A combined experimental and numerical investigation on the scaling laws for steel box structures subjected to internal blast loading, Int. J. Impact Eng. 102 (2017) 36–46.
[35] X. Kong, X. Li, C. Zheng, F. Liu, W.-g. Wu, Similarity considerations for scale-down model versus prototype on impact response of plates under blast loads, Int. J. Impact Eng. 101 (2017) 32–41.
[36] C. Zheng, X.S. Kong, W.G. Wu, S.X. Xu, Z.W. Guan, Experimental and numerical studies on the dynamic response of steel plates subjected to confined blast loading, Int. J. Impact Eng. 113 (2018) 144–160.
[37] W.E. Baker, Explosions in Air, University of Texas Press, Austin and London, 1973, pp. 150–167.
[38] G.S. Langdon, A. Ozinsky, S. Chung Kim Yuen, The response of partially confined right circular stainless steel cylinders to internal air-blast loading, Int. J. Impact Eng. 73 (2014) 1–14.
[39] AUTODYN Library, in Century Dynamics Incorporated, 2007. USA.
[40] Z. Zhang, C. Xiao, L. Chen, C. Wang, Y. Huang, Approximate scaling method of stiffened plate subjected to underwater explosion blast, J. Ship Mech. 14 (11) (2010) 1276–1283.